Adriana NEAG, Tudor BALAN - Verification of flow curve determination from plane strain compression tests - CIRP Journal of Manufacturing Science and Technology - Vol. 63, p.554-565 - 2025

A Neag, T Balan, Verification of flow curve determination from plane strain compression tests, CIRP J Manufacturing Science and Technology 63 (2025) 554-565, ISSN 1755-5817, doi.org/10.1016/j.cirpj.2025.11.005.

Verification of Flow Curve Determination from Plane Strain Compression Tests

Adriana Neag[1,2], Tudor Balan[1]*

[1] Arts et Metiers Institute of Technology, Université de Lorraine, LCFC, F-57070 Metz, France

[2] Dept of Materials Science and Engineering, Technical University, Cluj-Napoca 400641, Romania

Abstract

The work-hardening curve of sheet metals under large plastic strains can be extracted from the Plane Strain Compression Test (PSCT) using an analytical method that relies on several simplifying assumptions and correction factors (friction, boundary conditions, lateral spreading, tool geometry, yield criterion, anisotropy). This study rigorously assesses each of these correction factors using finite element simulations. Synthetic materials with predefined hardening laws are used to enable direct comparison between the reference curves and those extracted from simulated PSCTs. Dedicated simulation setups were developed to isolate the effect of each factor through progressive 2D and 3D configurations. The results show that the analytical method is generally valid when appropriate corrections are applied, with improved accuracy observed when using rounded tools with small radii under low-friction conditions. Recommendations for the selection of correction factors are provided to enhance the reliability of flow curves obtained through this method.

Keywords: Plane strain compression test (PSCT); sheet metal; large strain flow curve; finite element simulation; verification

* Corresponding author: Tel: +33.3.87.37.54.60; E-mail address: tudor.balan@ensam.eu

1. Introduction

The tensile test is commonly used to characterize the hardening behavior of sheet metals at room temperature, but the range of usable strains is limited to the uniform elongation. For high strength materials, this became a significant limitation [1]. In particular, finite element simulations of forming operations require hardening models capable of handling strains well beyond the uniform elongation. Uncontrolled extrapolation of tensile test data to higher strains can significantly affect predictions like springback or formability [2].

As a result, various alternative experimental methods were proposed to characterize sheet metals at larger strains. The hydraulic bulge test [3-11] is widely used since its standardization [12]. Other techniques, such as the stacked compression test [4-14], the simple shear test [15-20], the in-plane torsion test [21-29], and the plane strain compression test (PSCT) [30-34], allow access to higher strains due to their significantly lower stress triaxiality. Although not standardized, both academia and industry are using these experimental methods. Another approach involves conducting tensile tests on samples pre-strained through rolling, drawing, extrusion or other compressive processes [35-43]. The recently proposed Continuous Bending under Tension (CBT) test [41-46] was also used as a pre-straining method by Poulin *et al.* [47]. Hybrid experimental-numerical approaches have been developed to exploit the post-uniform elongation part of the tensile test [48-54]. Additionally, the in-plane bending test has been recently proposed to reach strains beyond uniform elongation in sheet metals [55-57]. Recent reviews and applications related to large strain hardening modeling and characterization can be found in [58-68]. A fundamentally different route involves physically-based crystal plasticity simulations of the material response up to relatively large strains, relying on texture measurements [69-74].

Originally, large strain characterization of sheet metals was motivated by the study of deformation mechanisms. However, with the development of finite element simulations of plastic deformation, the demand for accurate descriptions of material hardening at large strains has increased, with increasing expectations on accuracy. This necessitates a rigorous verification of the various assumptions inherent to the analytical approaches used to extract the material's flow curve from experimental tests [75], [76].

The plane strain compression test (PSCT), which is the focus of this study, presents several advantages: the testing setup involves a universal tension-compression machine with a dedicated die set, samples sizes are small, and postprocessing is analytical [39-41], [77-79]. This analytical flow curve extraction method was originally developed for hot rolling applications [32], [80], [81]. It was later applied to room-temperature sheet metal characterization by Becker *et al*. [82], who used rounded dies to delay fracture. Chermette *et al*. [83] refined this method by combining PSCT and uniaxial tensile test results, following the approach of [12].

The PSCT test configuration is illustrated in Fig. 1, along with the main notations. A rectangular sample of breadth b_0 and thickness h_0 is compressed between two dies of width w_0. The die edges can be either sharp or rounded, with radius r. In the latter case, the contact width between the dies and the sample evolves during the test. Typically, the axial force and displacement of the dies are recorded during the test.

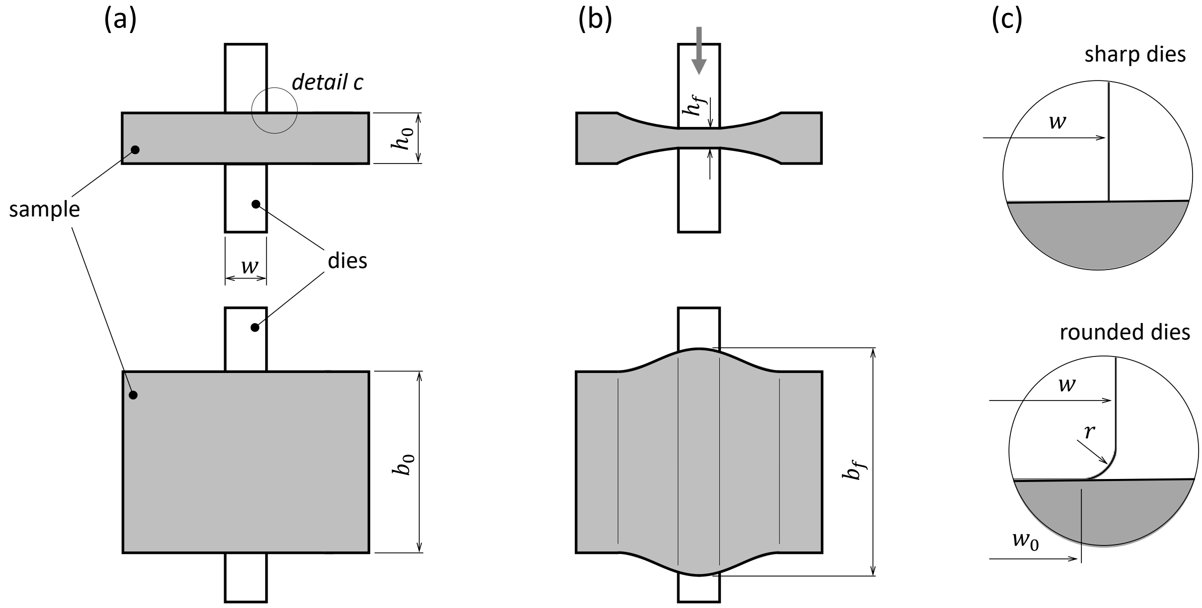

Fig. 1. Schematic representation of the plane strain compression test (PSCT) and notations: a) beginning of the test; b) end of the test; c) detail of the die edge for both sharp and rounded dies.

Inverse methods based on finite element (FE) simulations have been proposed to identify the parameters of a chosen hardening law [78], [84-87]. However, most authors use the analytical method to extract the flow curve from force-displacement data, without any assumption on the form of the hardening law [32]. This analytical approach relies on several simplifying assumptions, following the spirit of the slab method, leading to a number of correction terms that aim to compensate for the effects of friction (C_{fr}), boundary conditions (C_{BC}), lateral spreading (C_b), effective tool width (C_w), yield surface shape (C_{YS}), and anisotropy (C_{an}). These lead to the following expressions of the yield stress σ_y and the corresponding effective strain ε_e:

$$\sigma_y = \frac{|F|}{w_0 b_0} \frac{1}{C_b} \frac{1}{C_{fr}+C_{BC}} \frac{1}{C_w} \frac{1}{C_{YS}C_{an}} , \qquad (1)$$

$$\varepsilon_e = \left| ln \frac{h}{h_0} \right| C_{YS}C_{an} , \quad (2)$$

where F is the axial force acting on the upper die.

Expressions for the correction factors are well documented in the literature:

$$C_{fr} = \begin{cases} \frac{h}{\mu a}\left(\mathrm{e}^{\mu\frac{w}{h}} - 1\right) & \text{with Coulomb friction law} \\ 1 + \bar{m}\frac{w}{4h} & \text{with Tresca friction law} \end{cases}, \quad (3)$$

$$C_{BC} = \begin{cases} 0 & \text{for the free surface condition} \\ \frac{h}{4w} & \text{for the edge shear condition} \end{cases}, \quad (4)$$

$$C_b = 1 + \left(\frac{b_f}{b_0} - 1\right)\frac{h_0^m - h^m}{h_0^m - h_f^m} \text{ with } m = 0.5 \text{ for most materials}, \quad (5)$$

$$C_w = min\left(\begin{array}{c} 1 + \frac{2r}{w_0}cos\left[sin^{-1}\left(1 - \frac{h_0 - h}{2r}\right)\right], \\ \frac{w_0^2 + \sqrt{r^2(h+2r)^2\left(1+\frac{h_0^2}{w_0^2}+\frac{4hr}{w_0^2}\right)} + h(1+4r)}{w_0^2+(h+2r)^2} \end{array}\right), \quad (6)$$

$$C_{YS} = \begin{cases} \frac{2}{\sqrt{3}} & \text{for the von Mises yield surface} \\ 1 & \text{for the Tresca yield surface} \end{cases}. \quad (7)$$

The anisotropy correction factor C_{an} is computed according to [12]. For detailed explanations, the reader is referred to [83], who recently applied this procedure to a large number of sheet steels at room temperature. Their results, along with others in the literature, support PSCT as a credible alternative for determining flow curves of sheet metals at large strains (see Fig. 2). The edge shear condition has only been derived in the literature in the framework of Tresca's yield surface [88]; accordingly, condition (4) was derived in this work for von Mises plasticity, with the derivation provided in the Appendix.

The objective of this paper is to rigorously verify these correction terms, independently whenever possible, to validate the analytical flow curve extraction method. To the best of the authors' knowledge, such a study has not yet been conducted. Several of the correction terms have several variants, inconsistently used across the literature, as illustrated in Eqs. (3)-(7). Notably, flow curves extracted from the PSCT are reported to display relatively steeper hardening slopes at large strains compared to other tests [89]. Although the use of rounded tools increases the strain range achievable before fracture and yields seemingly accurate results [83], the acceptable or recommended range of die radii has not been investigated. This study aims to clarify these issues.

The remainder of the paper is structured as follows. The research methodology is presented in Section 2. Results are summarized in Section 3 and further discussed in Section 4. Conclusions are drawn in the final section.

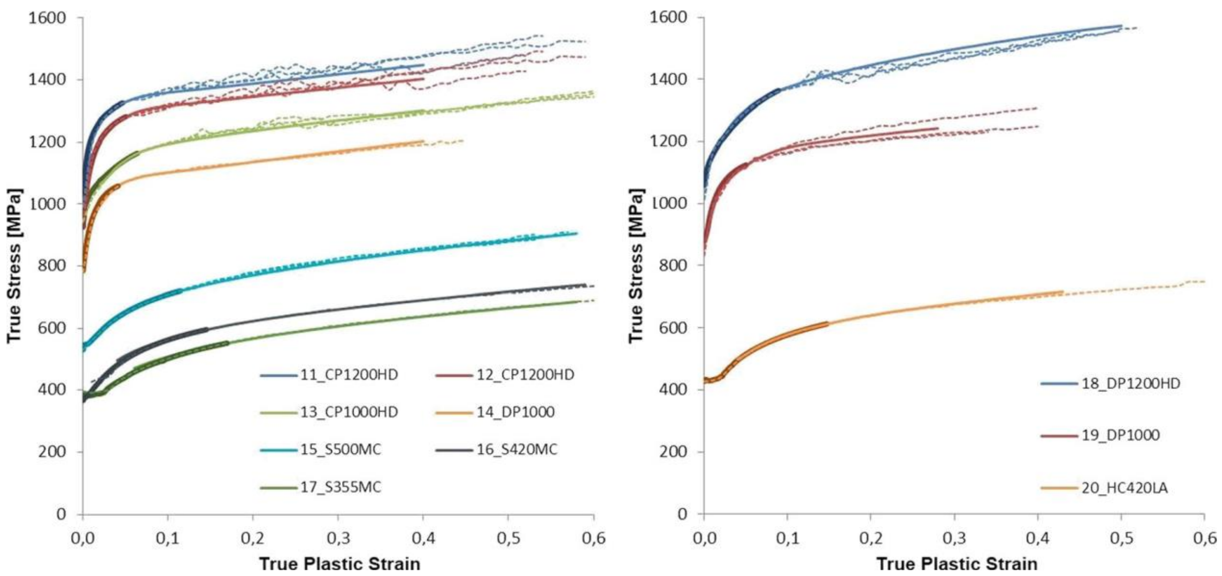

Fig. 2. Example of experimental validation of PSCT-based flow curves against bulge test experiments [83].

2. Investigation method

To independently isolate the influence of each correction factor introduced in Eq. (1), FE simulation of the PSCT was adopted as the primary investigation tool in this study. The material was modeled using von Mises plasticity with isotropic power-law hardening. Simulations were carried out using the Forge NxT 4.0 software. Particular care was taken to ensure numerical convergence and control of discretization errors.

The main output from the simulation was the evolution of the die force as a function of die stroke, mimicking the data collected in a physical PSCT experiment. The analytical flow curve extraction procedure detailed in [83] and based on Eqs. (1)-(7) was applied to this simulated force-displacement curve. The outcome of this procedure was a set of stress-strain pairs representing the derived flow curve, which was then compared against the known flow curve used as input in the simulation. This methodology is schematically illustrated in Fig. 3.

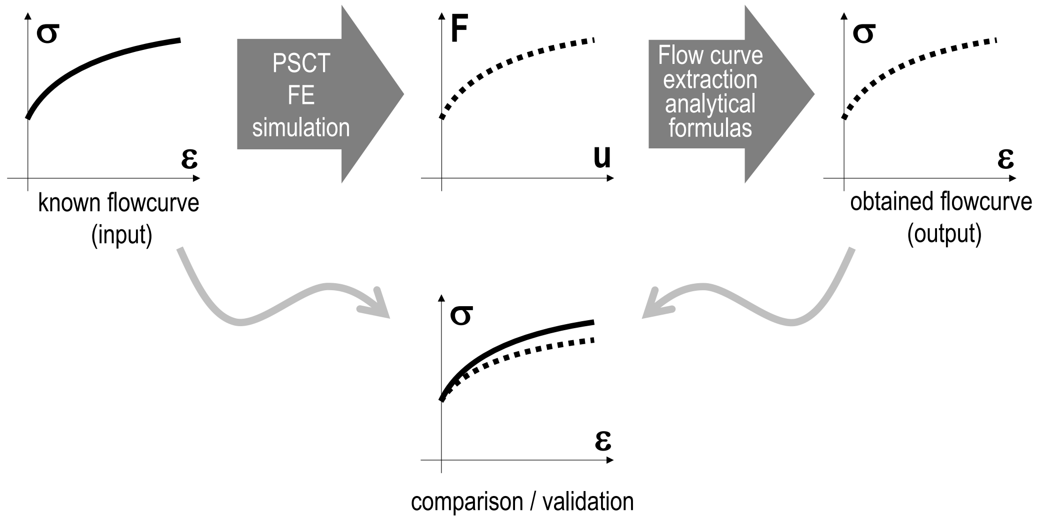

Fig. 3. Methodology flowchart for the numerical validation of correction terms in PSCT analysis.

A major advantage of this numerical validation approach is the availability of a perfectly known reference flow curve, whereas in experimental validation, the reference flow curve must itself be derived from an alternative experiment – often subject to its own assumptions and limitations. A second advantage lies in the ability to independently assess the influence of each correction term, which is hardly achievable in experiments. To this end, several simulation configurations were designed to isolate the effects of the various parameters influencing the flow curve extraction procedure, as shown in Fig. 4. Initial simulations were conducted in two dimensions to eliminate the influence of specimen breadth variation and to remain consistent with the plane-strain assumption underlying the analytical PSCT models. These simulations enabled investigation of the effects of the yield surface shape, friction, and edge shear, – both individually and in combination. The impact of die misalignment was also studied in 2D. Subsequently, rounded dies with different radii were simulated. To investigate the influence of specimen breadth increase and perform full-factor validation, 3D simulations were carried out as well.

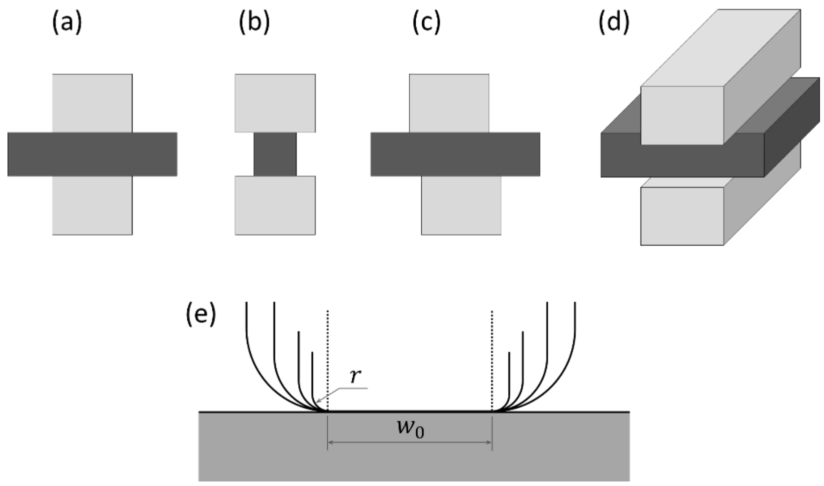

Fig. 4. Simulated PSCT configurations for correction term validation: a) reference configuration; b) reduced length configuration; c) misalignment configuration; d) 3D configuration. Configurations (a) and (d) were used with both sharp and rounded dies. e) Construction of rounded dies; sharp die geometry shown in dotted lines for reference.

The geometric parameters used in all simulations are summarized in Table 1 (see also Fig. 1). For the rounded die configurations, the initial die-sample contact width was maintained constant (equal to w_0), as shown in Fig. 4e.

Von Mises plasticity was used with a Swift-type hardening law of the form

$$\sigma_y = k(\varepsilon_0 + \varepsilon_e)^n \,, \quad (8)$$

where σ_y is the flow stress, ε_e is the equivalent strain, and k, n, ε_0 are material constants. A combined Coulomb-Tresca friction model was employed, as described in [90]. Three synthetic material datasets and several friction conditions were tested; all parameters are provided in Table 2, and the corresponding flow curves are shown in Fig. 5. The three materials were selected to have identical yield stress but varying hardening rates in both low and high strain regimes, enabling verification of the generality of the conclusions drawn. Material A was used for most simulations, while the three materials were used in the final verification stage.

Mesh convergence was verified for each configuration. A uniform mesh size of 0.025 *mm* was selected for 2D simulations and 0.1 *mm* for 3D simulations due to the significantly higher computational cost. In regions near the die-sample interface, the mesh was locally refined to 0.02 *mm* to capture contact effects accurately, since the contact surface area directly impacts the calculated force. The numerical volume variation due to remeshing was monitored remained inferior to 0.9% across all simulations.

The complete simulation matrix is summarized in Table 3. This progressive approach enabled isolated validation of each term Eq. (1), culminating in a global verification integrating all factors.

Table 1. Dimensions of the sample and dies used in the investigation, according to Figure 1.

Dimension	h_0	b_0	w_0	r
Value [mm]	2	25	5	0; 0.25; 0.5; 1; 1.5

Table 2. Material and friction model parameters used in the simulations.

Swift hardening law, Eq (8)				
Material	A	B	C	
k [MPa]	950	950	650	
n	0.2	0.1	0.2	
ε_0	0.013	0.00013	0.085	
Friction law, combined Tresca ($\overline{m}$) and Coulomb (μ), Eq (3)				
Friction level	high	medium	low	frictionless
$\overline{m}$	0.4	0.1	0.05	0
μ	0.2	0.05	0.02	0

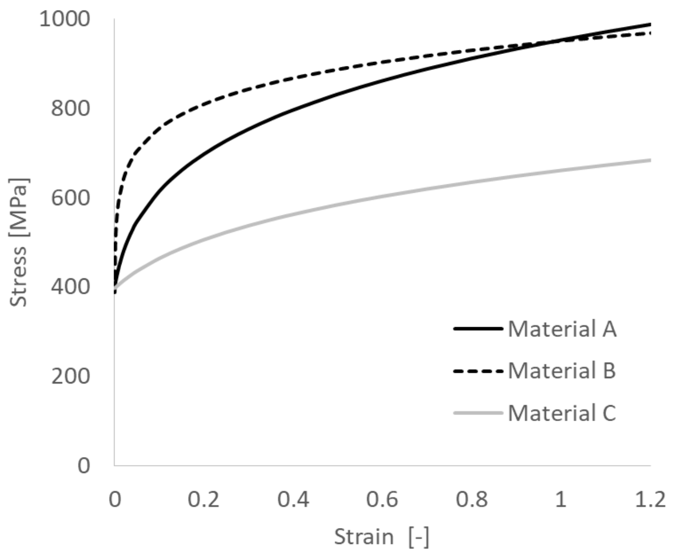

Fig. 5. Flow curves of synthetic materials A, B and C (see Table 2).

Table 3. Summary of simulations. For geometrical characteristics of the simulation configurations *a…d* refer to Fig. 4; configurations *a…c* are 2D while configuration *d* is 3D.

Confi-guration	Edge radius	material	friction	Required corrections					
				C_{YS}	C_{BC}	C_{fr}	C_b	C_w	C_{an}
b	-	A	-	×					
a	-	A	-	×	×				
a	-	A	low, med, high	×	×	×			
d	-	A	low	×	×	×	×		
a	0.25, 0.5, 1, 1.5	A	low	×	×	×		×	
d	0.5	A,B,C	low	×	×	×	×	×	×

3. Results

The core results of the investigation consist of flow curves extracted from FE simulations carried out under various configurations and combinations of material and friction parameters. These extracted curves were systematically compared to the reference flow curve. The analysis is organized as follows: Section 3.1 presents results obtained with sharp dies, which are the most commonly used in the literature. Section 3.2 addresses the case of rounded dies. Finally, Section 3.3 combines all correction terms for the three synthetic materials.

3.1. Validation of PSCT correction terms for sharp tools

The simplest PSCT configuration corresponds to a short specimen length, smaller than the die width, with frictionless contact conditions in a 2D plane strain simulation. Under such conditions, the geometry remained rectangular, and both strain and stress fields remain homogeneous even at large die strokes. The only parameter influencing the resulting die force is thus the material's constitutive law.

Fig. 6 shows the flow curves extracted using both the von Mises and Tresca yield surfaces – Eq. (7). As expected, the von Mises-based extraction matches the input flow curve precisely, while the Tresca-based extraction overestimates the flow stress by a factor of $2/\sqrt{3}$, expressing the ratio between the necessary yield pressure in plane strain for the two yield criteria. Although this result is anticipated due to the use of von Mises plasticity in the simulations themselves, it highlights the significant discrepancies that may arise between different isotropic yield criteria under certain loading conditions, particularly shear and plane strain compression.

In the context of isotropic BCC metals such as steel, von Mises plasticity is generally appropriate. However, it is noteworthy that flow curves derived using the Tresca yield surface have still demonstrated good accuracy in the literature, as seen in Fig. 2. This apparent paradox can be attributed to the anisotropy correction factor C_{an}, which also compensates for potential mismatches in the assumed isotropic yield surface. Their average correction factor of 1.14 is very close to $2/\sqrt{3}$, supporting this interpretation. To distinguish these two influences, two separate correction terms are used in Eq. (1): C_{YS}, which accounts for the adopted isotropic yield surface, and C_{an}, which corrects for material anisotropy. Throughout this work, the von Mises yield surface was adopted, and thus $C_{YS} = 2/\sqrt{3}$.

The 2D reference configuration was used, in frictionless conditions, to examine the impact of boundary conditions adopted at the edge $\partial\Omega$ of the computational domain Ω, as defined in the slab analysis of the PSCT (see Fig. 7). Most authors adopt a free surface condition, but Becker *et al.* [82] and later Chermette *et al.* [83] proposed incorporating an additional shear strain component due to the geometric variation at the die edge. This leads to a shear correction term C_{sh}, which complements the traditional friction correction term, as shown in Eqs. (1) and (3).

The frictionless 2D reference configuration is well-suited to isolate the effect of this boundary condition. Fig. 8a shows that both hypotheses – free surface and additional shear strain – result in slight deviations from the reference flow curve. The free surface assumption leads to an overestimation of the initial hardening slope, leading to a relatively higher flow curve, while the shear correction produces the opposite effect. These trends diminish and eventually reverse with increasing strain, causing the flow curves to intersect around a strain of 0.7-0.8 for Material A. For this material-geometry combination, both hypotheses offer comparable accuracy, with a slight advantage for the shear correction: the maximum errors were 5% without shear correction and 4% with it, remaining nearly constant up to strains of 0.1-0.15 before decreasing similarly.

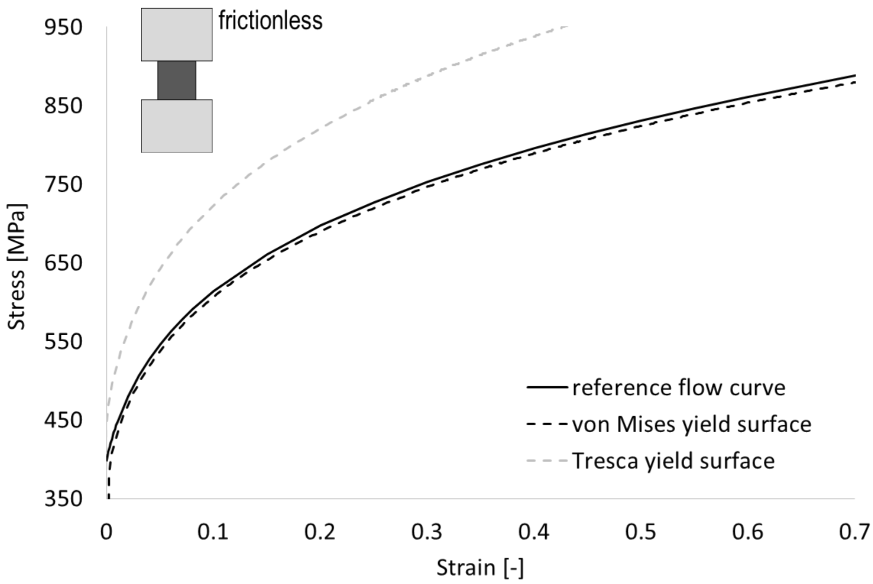

Fig. 6. Flow curves extracted from the 2D, frictionless, short-length configuration, using von Mises and Tresca yield surfaces, compared to the reference flow curve.

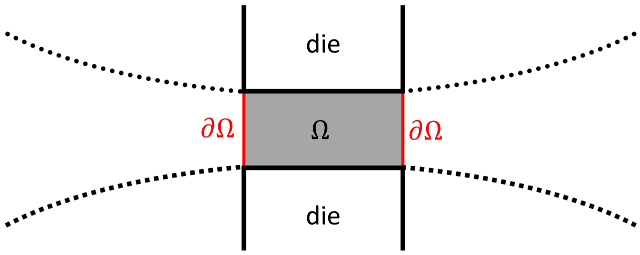

Fig. 7. Schematic representation of the PSCT slab analysis domain and its boundaries of concern. The gray area denotes the material volume considered in the calculation. Dotted lines indicate neglected zones.

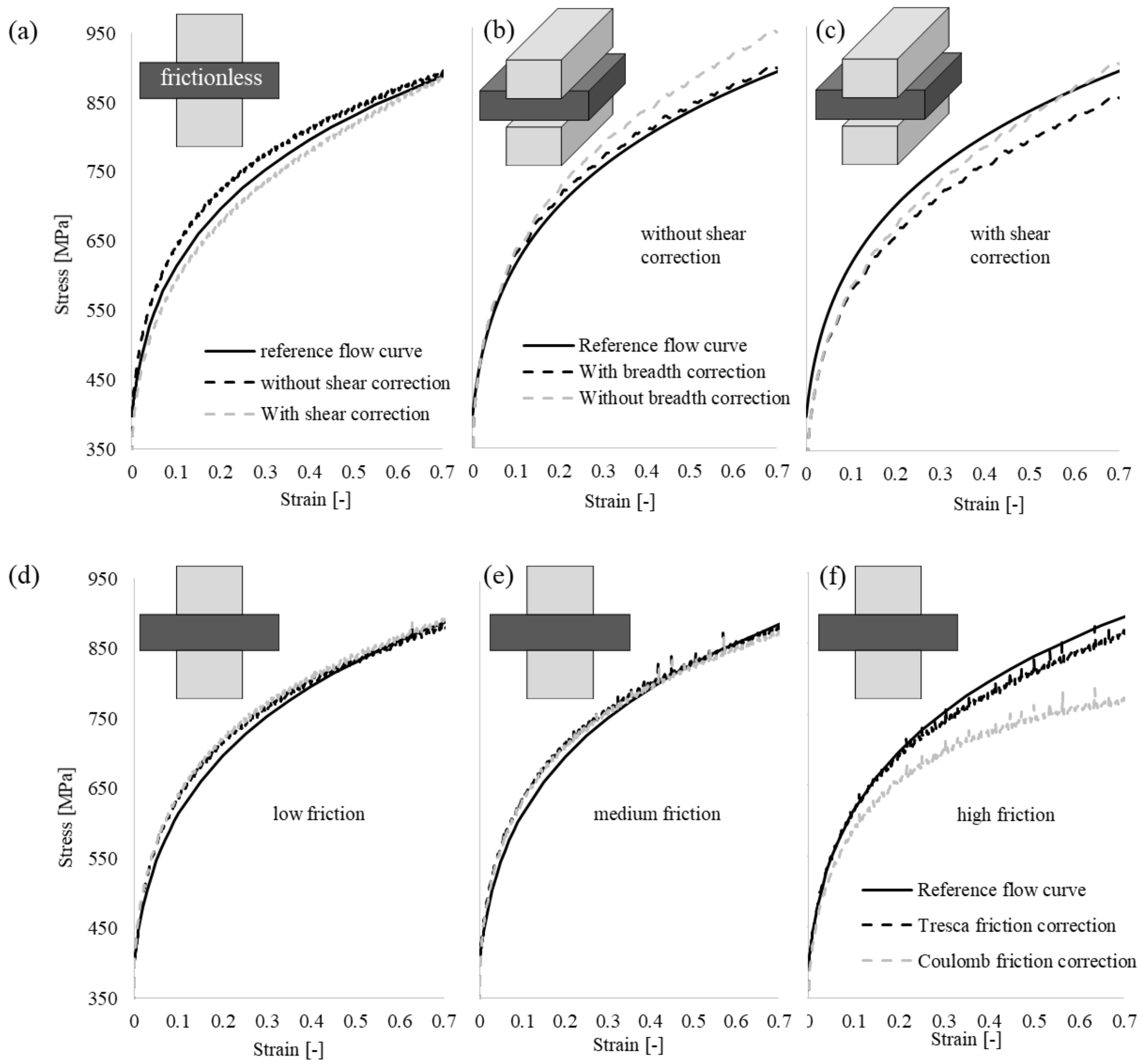

Fig. 8. Flow curves extracted for 2D and 3D PSCT configurations with sharp tools: (a) Validation of the shear correction term using the frictionless 2D reference configuration; (b)-(c) Validation of the breadth correction term in the 3D configuration in low friction condition, without and with shear correction, (d)-(f) verification of the friction correction term for low, medium, and high friction conditions.

Friction effects were then included in the 2D reference configuration. Correction terms for both Coulomb or Tresca friction models were applied. Fig. 8d-f presents the corresponding results under low, medium, and high friction conditions, which represent a range of typical lubrication scenarios. Since the friction coefficients were known in the simulation, they were also used for the correction terms. Although one could devise a combined Coulomb-Tresca correction term, this would be of limited value for real experiments, where friction models and coefficients are generally unknown or uncertain. Prior studies (e.g., [91]) have shown that Tresca and Coulomb-Tresca corrections yield very similar results. Hence, only the standard Coulomb and Tresca friction corrections were evaluated here. Note that we designate here the parameters of both friction models as “coefficients”, in the mathematical sense of the term, although in the literature the term “friction factor” is often preferred for the Tresca friction model.

The results show that the Tresca friction correction consistently outperforms the Coulomb correction and should therefore be preferred. Moreover, applying a friction correction consistently improves the accuracy of the extracted flow curve. However, the correction becomes less accurate as the friction coefficient increases, which highlights the importance of using excellent lubrication conditions in practice. Consequently, all subsequent simulations in this work were conducted under low friction conditions with the Tresca correction factor, unless stated otherwise. Interestingly, when the shear correction was also applied (Fig. 8f) the breadth correction no longer improved the result. Nevertheless, in both cases, the breadth correction led to a much better estimation of the hardening rate evolution. By contrast, the benefit of the shear correction becomes less clear outside the 2D simulation framework.

3.2. Validation of the effective tool width for rounded tools

Flow curves extracted from 2D PSCT simulations with the reference configuration and rounded dies are shown in Fig. 9a. When the die radius is small, the extracted curves show relatively low deviations from the reference, but the error increases with larger die radii. This trend suggests that keeping the die radius small helps reduce inaccuracies in the flow curve while still reaping the mechanical benefits of rounded die edges.

Additional insights are shown in Fig. 9b for a representative case with a die radius of 0.5 *mm*. Here, incorporating a variable effective tool width (ETW) successfully improves flow curve predictions at low strains, compared to results based on a constant tool width, which tended to overestimate the stress. This improvement, however, is subject to two limitations. First, as the die radius increases, the actual die-sample contact deviates more significantly from the assumed geometry, reducing the accuracy of the ETW estimation. Second, as strain approaches the range associated with uniform elongation, the extracted flow curve begins to show a reduced hardening slope relative to the reference. This trend also appeared in simulations using a constant tool width, indicating that the discrepancy is not exclusive to the ETW correction but likely inherent to the PSCT setup under these deformation conditions.

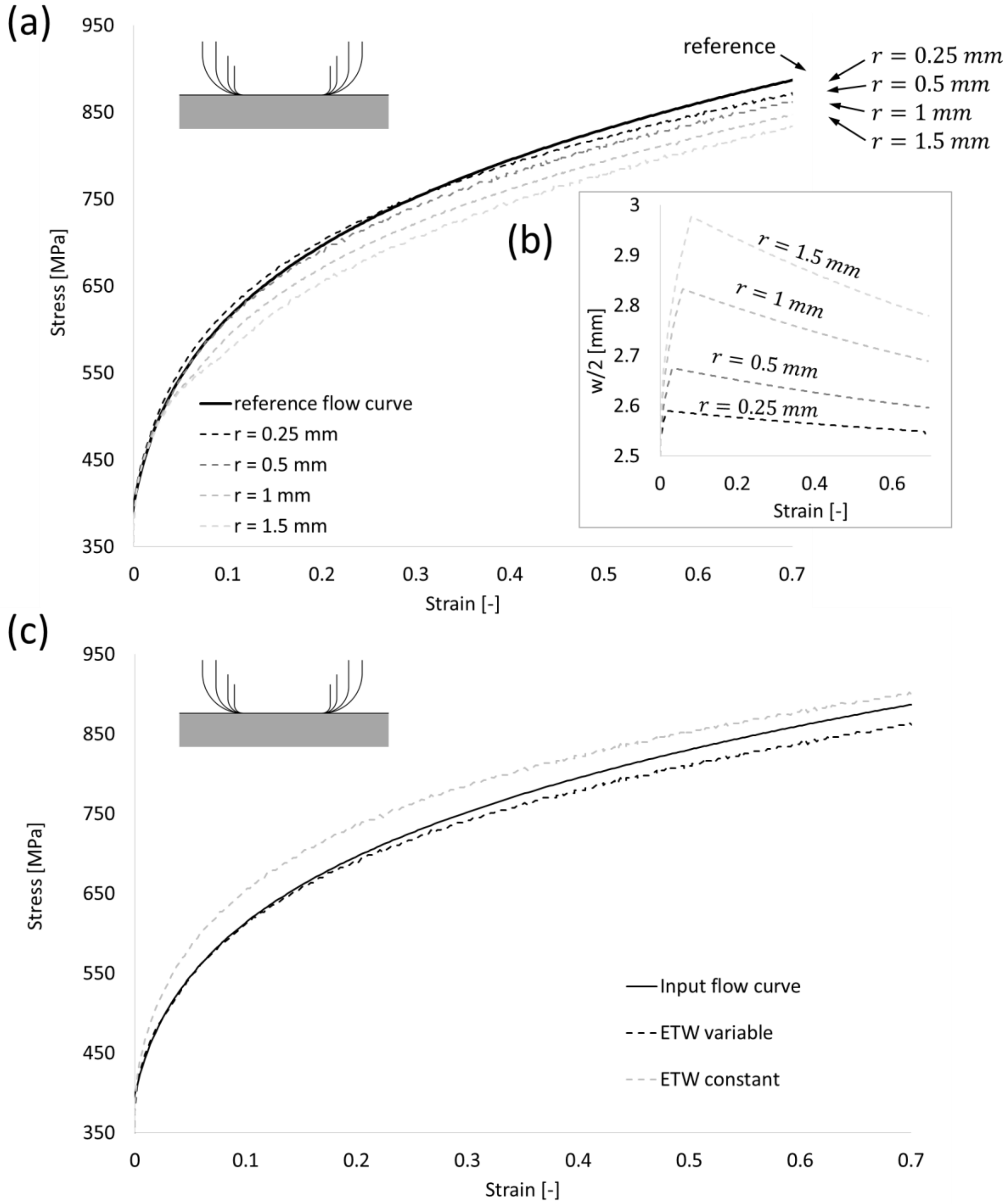

Fig. 9. Effect of rounded dies in 2D PSCT simulations (low friction, Tresca friction correction): a) stress-strain curves for various die radii; b) evolution of the effective tool width (ETW); c) flow curves extracted using a constant vs. variable ETW for a 0.5 *mm* die radius.

3.3. Combined effect of all corrections, including anisotropy correction

After individually evaluating the main correction terms, the full flow curve extraction procedure was applied to the complete 3D PSCT configuration with rounded dies and low friction conditions – representing the realistic experimental setup. Both the breadth correction and the Tresca friction correction were included in all cases, and three synthetic material parameter sets were considered. The results, shown in Fig. 10a-c, demonstrate that for this particular configuration, neither the tool width correction nor the shear correction significantly improves the accuracy of the extracted flow curves. The predictions were already very close to the reference curve without these corrections (Fig. 10a).

Finally, Fig. 10d-f display the flow curves obtained for materials A, B and C after applying the anisotropy correction. In all cases, the corrected flow curves intersect the reference curves at the true uniform elongation. At higher strain levels, the hardening slope tends to be slightly underpredicted when using a constant tool width, and slightly overpredicted when using a variable tool width. In both scenarios, however, the global accuracy is satisfactory. The shear correction, in contrast, results in a noticeable overestimation of the hardening slope, particularly at large strains, which degrades the quality of the flow curve extraction. This observation suggests that the shear correction may not be suitable in the context of 3D PSCT simulations with rounded tools.

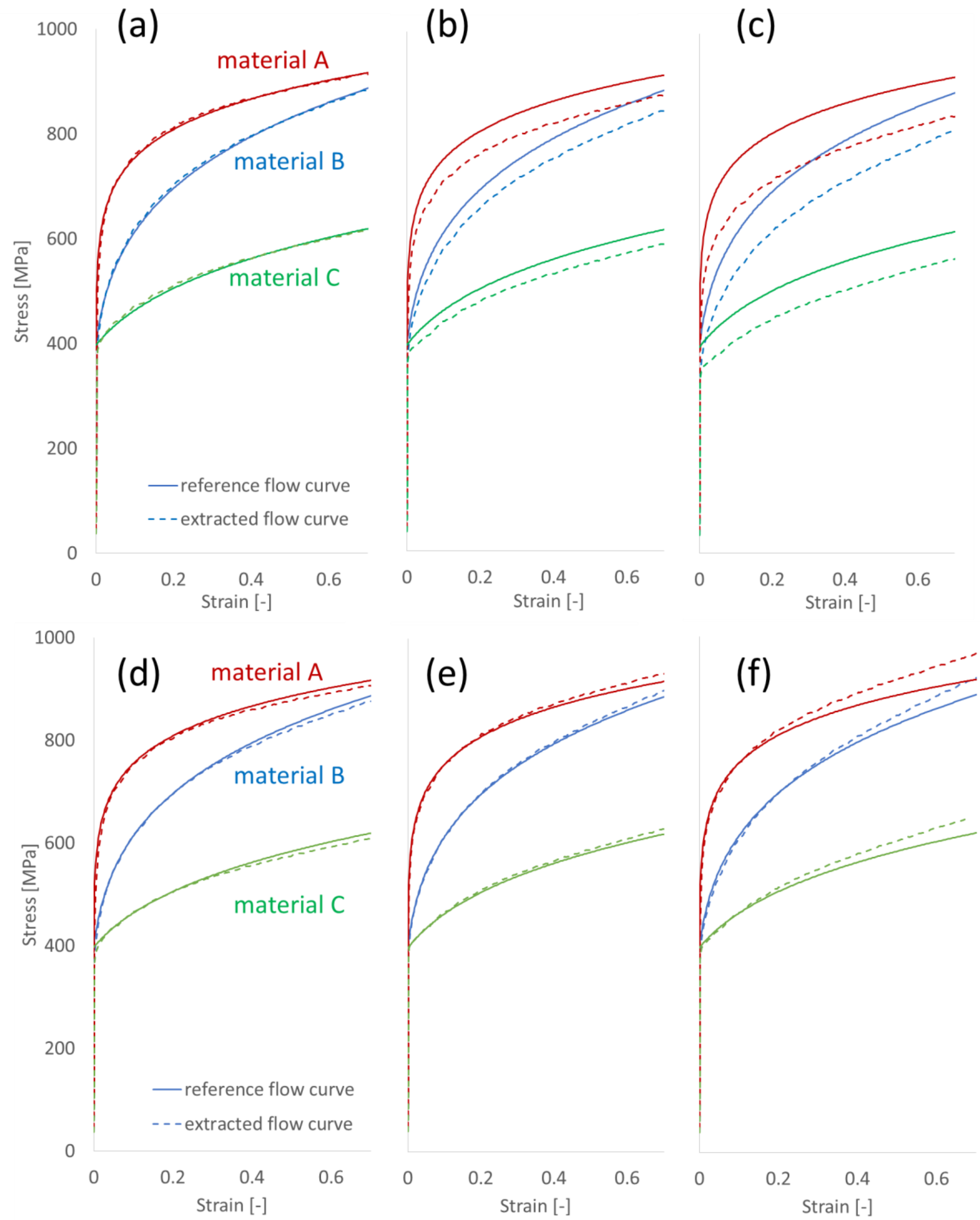

Fig. 10. Extracted flow curves for materials A, B and C in the 3D configuration with rounded tools: a) with constant tool width, b) with evolving tool width, c) with evolving tool width and shear correction. Extracted flow curves after applying anisotropy correction: d) constant tool width, e) evolving tool width, and f) evolving tool width with shear correction.

4. Discussion

The Tresca-based friction correction appeared as both significant and reliable. It is worth noting, however, that the friction correction assumes a constant friction coefficient through the test. In practice, due to the large contact pressures and significant sliding at the die-sample interface, lubrication conditions deteriorate during testing, leading to a likely increase in the effective friction coefficient. This variation is difficult to characterize experimentally. Therefore, in order to ensure the PSCT can be used for quantitative flow curve extraction at room temperature, maintaining optimal lubrication conditions is crucial to minimize frictional effects.

Regarding the hardening slope, most configurations and material combinations did not show significant deviations from the reference curve. Nevertheless, some correction terms had a distinct impact. The hardening slope tended to be underpredicted when using the friction correction, the free surface hypothesis, or in the presence of a tool misalignment (see Fig. 11). It was overpredicted when applying the shear correction. The anisotropy correction was effective at compensating for several types of error—not limited to true material anisotropy—but cannot simultaneously correct for both flow stress and hardening slope errors.

The friction correction showed high accuracy under idealized, known conditions in the simulations, supporting the systematic use of the Tresca friction correction. However, in experimental setups, the friction coefficient is uncertain and evolves throughout the test due to plastic deformation and interface changes. This evolving friction is likely a key factor contributing to the increased hardening slope observed in experimental PSCT data at large strains.

While the present investigation provides a detailed numerical validation of individual and combined correction terms, it is important to acknowledge certain limitations. First, the simulations were conducted under idealized conditions, with known and constant friction coefficients, perfect die alignment, and ideal isotropic material behavior. These assumptions were necessary to isolate and evaluate the influence of each correction term, but they do not fully capture the uncertainties and variability present in real experimental settings. In particular, the friction conditions in actual PSCT experiments are known to evolve during the test and may lead to stronger deviations in the extracted flow curve than those observed in this study. Second, although the numerical results are compared to analytical and literature-based references, no direct experimental validation was included. Future work should aim to confirm the conclusions using controlled experiments, especially to assess the real-world effectiveness of the proposed correction strategies. Finally, the combined application of multiple correction terms can sometimes lead to non-additive effects, depending on the specific test configuration. In certain cases, such as the simultaneous use of shear and tool width corrections in 3D simulations, the accuracy of the extracted flow curve was not improved and could even decrease.

The PSCT analysis makes few assumptions about the material's behavior. For anisotropic materials, the experimental confrontations from [83] – see also Figure 2 – showed excellent accuracy. However, it was implicitly assumed that the material obeys to the normality rule and does not exhibit tension-compression strength-differential effects or so-called anisotropic hardening effects. It is noteworthy that for materials that do not verify these assumptions, the PSCT alone will not be sufficient to completely characterize the hardening response, and the application of the methodology to post-process the PSCT for such materials becomes questionable.

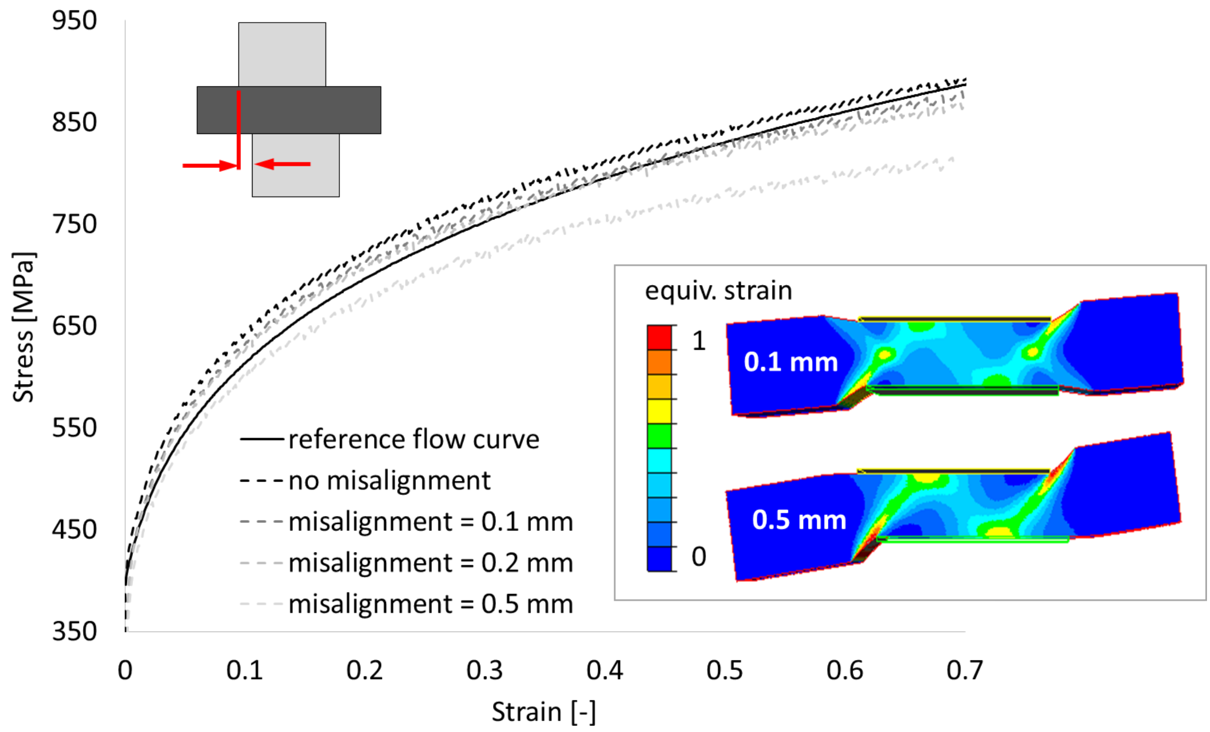

Fig. 11. Flow curves extracted from 3D simulations material A under low friction conditions, for various levels of tool misalignment.

5. Conclusions

The plane strain compression test was investigated through finite element simulations, and the material's flow curve was extracted using an analytical post-processing procedure. Several conclusions can be drawn regarding the accuracy and relevance of the correction terms involved, in view of their application to experimental PSCT analysis.

The correction for breadth increase should always be applied, as well as the Tresca friction correction, both of which proved to be impactful and accurate. In contrast, the shear correction did not improve the results in realistic 3D configurations and can therefore be omitted in such cases.

For the use of rounded tools, the die radius should be kept below 0.5 mm to preserve the accuracy of the analytical flow curve extraction. Larger radii lead to a noticeable degradation in accuracy. Furthermore, the computation of the effective tool width did not lead to improved results in the 3D configurations and can therefore be discarded.

Finally, the apparent hardening slope of the extracted flow curves was not significantly affected by the studied configurations and materials, except when applying the shear and tool width corrections. Therefore, the increase in the hardening slope observed experimentally at large strains is likely due to other factors not present in the simulation, such as evolving friction conditions during the test.

6. Appendix: Calculation of the shear correction using the von Mises yield criterion

In the available literature [83, 88], the edge shear correction term was only calculated in the framework of the Tresca yield surface, which usually leads to simpler (linear) equations as compared to the von Mises yield criterion. Thus, in this work the shear correction term was analytically derived in the framework of von Mises plasticity.

The boundary $\partial\Omega$ (see Fig. 7) is considered as a free edge in most analytical approaches. However, Ismar and Mahrenholtz [88] inferred that the geometry of the sample at this transition point, exhibiting a variation in thickness, could indicate that a local shear instantaneously occurs when the material crosses this boundary, as illustrated in Fig. 12. Since the demonstration was made assuming a Tresca plasticity criterion, the solution is derived here for a von Mises material.

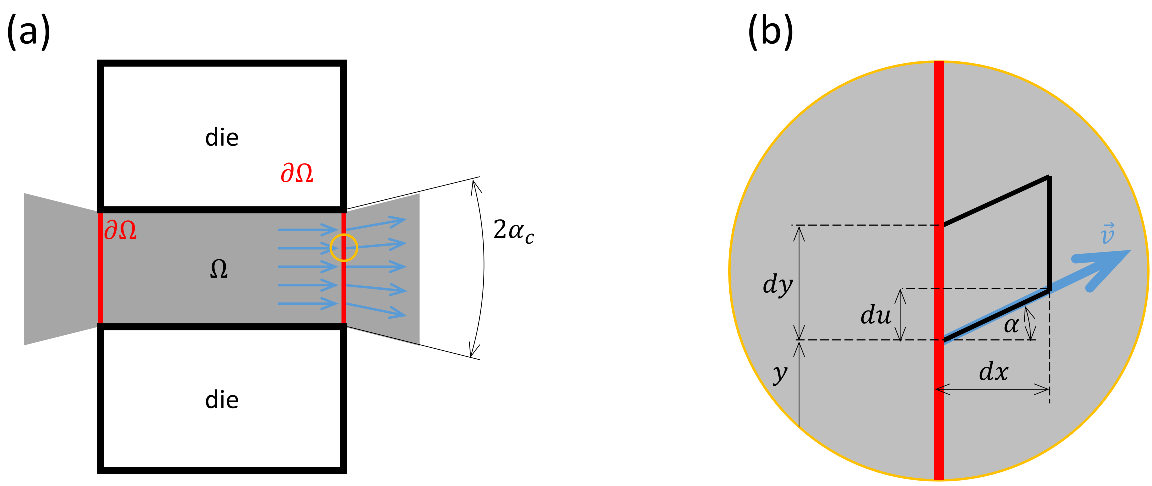

Fig. 12. Extended slab method analysis, considering an additional material shearing when crossing the boundary $\partial\Omega$; a) schematic representation and b) infinitesimal volume element after crossing the boundary and notations used in the demonstration.

A simple shear stress tensor is assumed at a material point crossing the border

$$\boldsymbol{\sigma} = \begin{bmatrix} 0 & \sigma_{xy} & 0 \\ \sigma_{xy} & 0 & 0 \\ 0 & 0 & 0 \end{bmatrix}, \quad (9)$$

and the dissipated energy per unit volume associated to this stress state writes

$$dW = 2\sigma_{xy}\varepsilon_{xy} = \sigma_{xy}\gamma_{xy}. \quad (10)$$

A linear velocity field is assumed that allows to calculate the shear strains as

$$\gamma_{xy} = \frac{du}{dx} = tan(\alpha) = \frac{v_y}{v_x} = tan(\alpha_c) \cdot \frac{2y}{h}, \quad (11)$$

while the shear stress can be related to the equivalent stress

$$\sigma_{xy} = \frac{\overline{\sigma}^{vM}}{\sqrt{3}}. \quad (12)$$

Finally, the dissipated energy per unit volume

$$dW = \sigma_{xy}\gamma_{xy} = \frac{\overline{\sigma}^{vM}}{\sqrt{3}} tan(\alpha_c) \frac{2y}{h} \quad (13)$$

can be integrated over the volume $b \cdot h \cdot dx$ of the two $\partial\Omega$ boundaries (left and right):

$$W = 2\int_{-\frac{h}{2}}^{\frac{h}{2}} dW\, b\, dx\, dy = 4\int_{0}^{\frac{h}{2}} dW\, b\, dx\, dy = \frac{8}{\sqrt{3}} \frac{\overline{\sigma}^{vM}}{h} b\, tan(\alpha_c) dx \int_{0}^{\frac{h}{2}} y\, dy. \quad (14)$$

Finally,

$$W = \frac{\overline{\sigma}^{vM}}{\sqrt{3}} bh\, tan(\alpha_c) dx. \quad (15)$$

This additional energy has to be provided by an increase of the σ_y stress component from the tool on the upper surface. The infinitesimal displacement of the tool dh corresponding to the ejection of an infinitesimal slab of width dx through boundary $\partial\Omega$ can be determined by volume conservation:

$$dV = \frac{w}{2} bdh = hbdx \;\; \Rightarrow \;\; dh = \frac{2h}{w} dx. \qquad (16)$$

By equalizing the shear energy with the additional energy provided by the tool,

$$\varDelta F\ dh = \varDelta\sigma_y\ b \frac{w}{2} dh = \frac{bh\overline{\sigma}^{vM}}{\sqrt{3}} tan(\ \alpha_c) dx, \ \ (17)$$

the increase in axial stress can be calculated as

$$\varDelta\sigma_y = \frac{\overline{\sigma}^{vM}}{\sqrt{3}} tan(\ \alpha_c) = \frac{\overline{\sigma}^{vM}}{\sqrt{3}} \frac{h}{2w} (18)$$

which was used to define the edge shear correction term in Eqs. (1) and (4). It is noteworthy that this shear correction term is form-identical whether one uses the von Mises or the Tresca yield criterion, provided that the yield surface shape factor (C_{YS}) is updated accordingly. For the detailed calculation of $tan(\ \alpha_c)$ the reader is referred to [83].

7. Acknowledgements

The second author is grateful to Klaus Unruh and Ilya Peshekhodov from Faurecia Autositze GmbH, Hannover, Germany, for initiating him to the PSCT and providing the original developments.

8. Data statement

For interested readers, data can be provided on request.

9. Author contributions: CRediT

Adriana Neag: Data curation, Formal analysis, Investigation, Visualization, Writing – original draft, Writing – review and editing; Tudor Balan: Conceptualization, Methodology, Supervision, Validation, Writing – original draft, Writing – review and editing.

10. Funding sources

This research did not receive any specific grant from funding agencies in the public, commercial, or not-for-profit sectors.

11. References

[1] X. Lemoine, R. Munier, X. Bellut, A robust identification protocol of flow curve adjusting parameters using uniaxial tensile curve, Mater. Res. Proc. 41 (2024) 2210 – 2219. https://doi.org/10.21741/9781644903131-243.

[2] M. Mohammadi, A.P. Brahme, R.K. Mishra, K. Inal K, Effects of post-necking hardening behavior and equivalent stress–strain curves on the accuracy of M–K based forming limit diagrams, Comput. Mater. Sci. 85 (2014) 316–323. https://doi.org/10.1016/J.COMMATSCI.2014.01.017.

[3] J. Mulder, H. Vegter, H. Aretz, S. Keller, A.H. van den Boogaard, Accurate deter-mination of flow curves using the bulge test with optical measuring systems. J. Mater. Process. Technol. 226 (2015) 169–187. https://doi.org/10.1016/J.JMATPROTEC.2015.06.034.

[4] M. Rossi, A. Lattanzi, L. Morichelli, J.M.P. Martins, S. Thuillier, A. Andrade-Campos, S. Coppieters, 2022. Testing methodologies for the calibration of advanced plasticity models for sheet metals: A review. Strain. 58, e12426. https://doi.org/10.1111/str.12426.

[5] Z. Wang, Z. Wang, Effects of non-uniform pressure on the deformation and instability of the sheet in flexible-die bulge forming, Int. J. Adv. Manuf. Tech. 135 (2024) 2571–2596. https://doi.org/10.1007/s00170-024-14624-2.

[6] F. Kharrat, M. Khlif, L. Hilliou, J.A. Covas, M. Haboussi, C. Bradai, Application of the bulge test combined with 3D-DIC for biaxial characterization of PLA films and defect detection, J. Plast. Film Sheeting. 39 (2023): 447–469. https://doi.org/10.1177/87560879231186142.

[7] M. Rossi, A. Lattanzi, F. Barlat, J.-H. Kim, 2022. Inverse identification of large strain plasticity using the hydraulic bulge-test and full-field measurements, Int. J. Solids. Struct. 242(4),111532. https://doi.org/10.1016/j.ijsolstr.2022.111532.

[8] L. Yuan, Q. Luo, K. Chen, 2023. Hydraulic bulge test instabilities of anisotropic materials, Int. J. Solids. Struct. 267, 112145. https://doi.org/10.1016/j.ijsolstr.2023.112145.

[9] A. Boyer, N. Demazel, J. Coër, M. Carin, H. Laurent, M.C. Oliveira, 2023. A novel hydraulic bulge test in hot forming conditions, J. Mater. Process. Technol. 316, 117917. https://doi.org/10.1016/j.jmatprotec.2023.117917.

[10] V.K. Barnwal, S.-Y. Lee, J. Choi, J.-H. Kim, F. Barlat, 2021. On the fracture characteristics of advanced high strength steels during hydraulic bulge test, Int. J. Mech. Sci. 190, 106032. https://doi.org/10.1016/j.ijmecsci.2020.106032.

[11] K. Chen, 2020. A general and unified theory of the kinematic relationships in bulge tests, J. Mech. Phys. Solids. 143, 104086. https://doi.org/10.1016/j.jmps.2020.104086.

[12] ISO 16808, 2014. Metallic materials - Sheet and strip - Determination of biaxial stress-strain curve by means of bulge test with optical measuring systems. International Organization for Standardization.

[13] Y. Tozawa, M. Nakamura, Methods for testing in-line compression of sheets. Journal of the Japan Society for Technology of Plasticity. 1967; 8: 444–448.

[14] Coppieters S, Jackel M, Kraus C, Kuwabara T, Barlat F. Influence of a Hydro-static Pressure Shift on the Flow Stress in Sheet Metal, Procedia Manuf. 47 (2020) 1245–1249. https://doi.org/10.1016/j.promfg.2020.04.196.

[15] T. Kuwabara, R. Tachibana, Y. Takada, T. Koizumi, S. Coppieters, F. Barlat, Effect of hydrostatic stress on the strength differential effect in low-carbon steel sheet, Int. J. Mater. Form. 15. 13 (2022). https://doi.org/10.1007/s12289-022-01650-2.
[16] Y. An, W. Spanjer, T. Chezan, J. Heijne, 2023. Investigating deformation and work hardening behaviour of stacked sheet metal specimens in compression test: Influence of friction and interfacial shear resistance. J. Mater. Process. Technol. 321, 118145. https://doi.org/10.1016/j.jmatprotec.2023.118145.
[17] Y.G. An, H. Vegter, Analytical and experimental study of frictional behaviour in through-thickness compression test, J. Mater. Process. Technol. 160 (2005) 148–155. https://doi.org/10.1016/j.jmatprotec.2004.05.026.
[18] M. Merklein, A. Kuppert, A method for the layer compression test considering the anisotropic material behaviour, Int. J. Mater. Form. 2 (2009) 483–486. https://doi.org/10.1007/s12289-009-0592-8.
[19] M. Kraus, M. Lenzen, M. Merklein, 2021. Contact pressure-dependent friction characterization by using a single sheet metal compression test. Wear. 476, 203679. https://doi.org/10.1016/j.wear.2021.203679.
[20] D.G. Szőke, M.L. Kölüs, R. Borbély, G.J. Béres, Capability testing of layered specimens in plane strain compression method, Lecture Notes in Mechanical Engineering. 2023; 363 – 372. DOI:10.1007/978-3-031-40920-2_38.
[21] E.F. Rauch, The Flow Law of Mild Steel under Monotonic or Complex Strain Path, Solid State Phenom. 23-24 (1992) 317–333. https://doi.org/10.4028/www.scientific.net/SSP.23-24.317.
[22] G. Vincze, E.F. Rauch, J.J. Gracio, F. Barlat, A.B. Lopes, A comparison of the mechanical behaviour of an AA1050 and a low carbon steel deformed upon strain reversal, Acta Materialia. 53(2005) 1005–1013. https://doi.org/10.1016/j.actamat.2004.10.046.
[23] S. Thuillier, P.Y. Manach, Comparison of the work-hardening of metallic sheets using tensile and shear strain paths, Int. J. Plast. 25 (2009) 733 – 751. https://doi.org/10.1016/j.ijplas.2008.07.002.
[24] S. Bouvier, N. Benmhenni, W. Tirry, F. Gregory, M.E. Nixon, O. Cazacu, L. Rabet, Hardening in relation with microstructure evolution of high purity α-titanium deformed under monotonic and cyclic simple shear loadings at room temperature, Mat. Sci. Eng. A. 535 (2012) 12–21. https://doi.org/10.1016/j.msea.2011.12.033.
[25] P.G. Gruber, J. Lekue, L. Wagner, T. Gross, S. Sieberer, M. Schagerl, 2024. Error analysis of deformation assumptions for the in-plane torsion test of sheet metal. Int. J. Solids Struct. 301, 112945. https://doi.org/10.1016/j.ijsolstr.2024.112945.
[26] J. Louge, R. Munier, C. Doudard, S. Calloch, B. Weber, 2021. Two new in-plane torsion tests for the investigation of self-heating under pure shear cyclic loading. Int. J. Fatigue. 149, 106256. https://doi.org/10.1016/j.ijfatigue.2021.106256.
[27] V. Grolleau, C.C. Roth, D. Mohr, 2022. Design of in-plane torsion experiment to characterize anisotropic plasticity and fracture under simple shear. Int. J. Solids Struct. 236-237, 111341. https://doi.org/10.1016/j.ijsolstr.2021.111341.
[28] X. Colon, V. Grolleau, B. Galpin, C.C. Roth, D. Mohr, 2024. In-plane Torsion Tests, Toward Large Strains Under Monotonic and Cyclic Loading of Sheet Metals. Lecture Notes in Mechanical Engineering. 754 – 763. https://doi.org/10.1007/978-3-031-42093-1_73.
[29] H. Traphöner, T. Clausmeyer, A.E. Tekkaya, 2021. Methods for measuring large shear strains in in-plane torsion tests. J. Mater. Process. Technol. 287, 116516. https://doi.org/10.1016/j.jmatprotec.2019.116516.
[30] N. Sae-Eaw, Y. Aue-U-Lan, Mechanical property determination for combined sheet and bulk metal forming process by plane strain compression test, Mater. Today Proc. 5(2018) 9376–9383. https://doi.org/10.1016/j.matpr.2017.10.113.

[31] A.B. Watts, H. Ford, An experimental investigation of the yielding of strip between smooth dies, Proceedings / Institution of Mechanical Engineers. 167 (1953) 448-464.
[32] M.S. Loveday, G.J. Mahon, B. Roebuck, A.J. Lacey, E.J. Palmiere, C.M. Sellars, M.R. von der Winden, Mat. High Temp. 23 (2006) 85-118. https://doi.org/10.1179/mht.2006.006.
[33] Y. Xiao, W. Zeng, R. Jia, B. Wang, Y. Dai, 2025. Mechanisms of slip modes and texture inheritance in Ti60 alloy during plane strain compression: Insights from texture evolution and regulation. J. Alloys Compd. 1013, 178579. https://doi.org/10.1016/j.jallcom.2025.178579.
[34] P.H. Silva, D.B. Santos, P.R. Cetlin, P. Henrique, R. Pereira, 2023. Strain partitioning in a dual-phase steel under plane strain compression. Mater. Sci. Eng. 862, 14447. https://doi.org/10.1016/j.msea.2022.144471.
[35] B. Wang, P. Zhang, Q.Q. Duan, Z.J. Zhang, H.J. Yang, J.C. Pang, Y.Z. Tian, Y.W. Li, Z.F. Zhang, High-cycle fatigue properties and damage mechanisms of pre-strained Fe-30Mn-0.9C twinning-induced plasticity steel, Mater. Sci. Eng. A. 679 (2017) 258-271. https://doi.org/10.1016/j.msea.2016.10.043.
[36] F. Kolpak, H. Traphöner, O. Hering, A.E. Tekkaya, Large strain flow curves of sheet metals by sheet extrusion, CIRP Ann. Manuf. Technol. 70 (2021) 247–250. https://doi.org/10.1016/j.cirp.2021.03.023.
[37] W. Tirry, S. Bouvier, N. Benmhenni, W. Hammami, A.M. Habraken, F. Coghe, D. Schryvers, L. Rabet, Twinning in pure Ti subjected to monotonic simple shear deformation, Mater. Charact. 72 (2012) 24–36. https://doi.org/10.1016/j.matchar.2012.07.001.
[38] S. Kumar, M. Panchal, A.N. Gandi, L. Kaushik, S.-H. Choi, J.Singh, Investigation of tensile twinning on texture and microstructure evolution of Mg-3Al-1Zn-1Ca alloy under in-plane shear deformation, J. Magnes. Alloys. 13 (2025) 1815–1828. https://doi.org/10.1016/j.jma.2025.02.017.
[39] M. Panchal, L. Kaushik, R. Kottan Renganayagalu, S.-H. Choi, J. Singh, 2024 Microstructure and texture evolution in AZX311 Mg alloy during in-plane shear deformation. J. Alloys Compd. 999, 174977. https://doi.org/10.1016/j.jallcom.2024.174977.
[40] Z. Marciniak, Influence of the sign change of the load on the strain hardening curve of a copper test piece subject to torsion, Archiwum Mechaniki Stosowanej. 13(1961) 743–752.
[41] A.E. Tekkaya, K. Pöhlandt, K. Lange, Determining stress-strain curves of sheet metal in the plane torsion test, CIRP Ann.-Manuf. Technol. 31 (1982) 171–174. https://doi.org/10.1016/S0007-8506(07)63291-0.
[42] G. Langford, M. Cohen, Strain hardening of iron by severe plastic deformation, Transactions of the ASM. 62 (1969) 623–638.
[43] G. Venet, C. Baudouin, C. Pondaven, R. Bigot, T. Balan, Parameter identification of 42CrMo4 steel hot forging plastic flow behaviour using industrial upsetting presses and finite element simulations, Int. J. Mater. Form. 14 (2021) 929–945. https://doi.org/10.1007/s12289-020-01609-1.
[44] W.C. Emmens, A.H. van den Boogaard, Incremental forming by continuous bending under tension—An experimental investigation, J. Mater. Process. Technol. 209 (2009) 5456–5463. https://doi.org/10.1016/j.jmatprotec.2009.04.023
[45] H. Long, S. Ai, F. Tian, B. Lu, J. Chen, H. Ou, A New Test Method for Sheet Metal Deformation subject to Tension under Cyclic Bending and Compression (TCBC). 2021; In: Daehn G, Cao J, Kinsey B, Tekkaya E, Vivek A, Yoshida Y. (eds) Forming the Future. The Minerals, Metals & Materials Series. Springer, Cham. https://doi.org/10.1007/978-3-030-75381-8_37.
[46] J.F.A. Pereira, P.A. Prates, M.C. Butuc, G. Vincze, Numerical study on continuous-bending-under-tension of 3rd generation steel, Metals. 15 (2025) 138. https://doi.org/10.3390/met15020138.

[47] C.M. Poulin, T.J. Barrett, M. Knezevic, Inferring post-necking strain hardening behavior of sheets by a combination of continuous bending under tension testing and finite element modeling, Exp. Mech. 60 (2020) 459–473. https://doi.org/10.1007/s11340-019-00577-1.

[48] S. Coppieters, S. Cooreman, H. Sol, P. van Houtte, D. Debruyne, Identification of the post-necking hardening behaviour of sheet metal by comparison of the internal and external work in the necking zone, J. Mater. Process. Technol. 211(2011) 545–552. https://doi.org/10.1016/j.jmatprotec.2010.11.015.

[49] B. Starman, T. Pepelnjak, A. Maček, M. Halilovič, S. Coppieters, 2025. Inverse calibration of out-of-plane shear anisotropy parameters of sheet metal. Int. J. Solids Struct. 313, 113313. https://doi.org/10.1016/j.ijsolstr.2025.113313.

[50] B. Chen, B. Starman, M. Halilovič, L.A. Berglund, S. Coppieters, Finite element model updating for material model calibration: A Review and Guide to Practice, Archives of Computational Methods in Engineering. 32(2025) 2035–2112. https://doi.org/10.1007/s11831-024-10200-9.

[51] S. Sueki, A. Ishii, S. Coppieters, A. Yamanaka, 2023. Inverse characterization of a material model using an ensemble-based four-dimensional variational method. Int. J. Solids Struct. 279, 112350. https://doi.org/10.1016/j.ijsolstr.2023.112350.

[52] E. Sakaridis, C.C. Roth, B. Jordan, D. Mohr, 2024. Post-Necking full-field FEMU identification of anisotropic plasticity from flat notched tension experiments. Int. J. Solids Struct. 305, 113076. https://doi.org/10.1016/j.ijsolstr.2024.113076.

[53] B. Jordan, V. Grolleau, D. Mohr, 2023. Using surround DIC to extract true stress–strain curve from uniaxial tension experiments. Int. J. Solids Struct. 268, 112171. https://doi.org/10.1016/j.ijsolstr.2023.112171.

[54] B. Starman, B. Chen, A. Maček, Y. Zhang, M. Halilovič, S. Coppieters, 2025, Characterising through-thickness shear anisotropy using the double-bridge shear test and finite element model updating. Materials. 18(10), 2220. https://doi.org/10.3390/ma18102220.

[55] S. Naseem, E.S. Perdahcıoğlu, H.J.M. Geijselaers, A.H. van den Boogaard, A new in-plane bending test to determine flow curves for materials with low uniform elongation, Exp. Mech. 60 (2020) 1225–1238. https://doi.org/10.1007/s11340-020-00621-5.

[56] M.M. Khalilabad, E.S. Perdahcıoğlu, E.H. Atzema, A.H. van den Boogaard, An in-plane bending test to characterize edge ductility in high-strength steels, J. Mater. Eng. Perform. 32(2023), 1892–1904. https://doi.org/10.1007/s11665-022-07202-8.

[57] A. Narayanan, R. George, C. Butcher, 2025. Uniaxial fracture and plastic anisotropy characterization of sheet metals using the in-plane bending test. Eng. Fract. Mech. 325, 111333. https://doi.org/10.1016/j.engfracmech.2025.111333.

[58] J. Wang., H. Jia, M. Wu, A. Pi, F. Huang, Z. Wang, F. Hao, 2025. Coupling effect of stress triaxiality and Lode angle over a wide range on the ductile fracture behavior and mechanism of high-strength steel 30CrMnSiNi2MoVE. Eng. Fract. Mech. 325, 111302. https://doi.org/10.1016/j.engfracmech.2025.111302.

[59] L.F. Folle, T.N. Lima, M.P.S. Santos, B. Callegari, B.C.D.S. Silva, L.G.S. Zamorano, R.S. Coelho, 2024. A review on sheet metal forming behavior in high-strength steels and the use of numerical simulations. Metals. 14(12), 1428. https://doi.org/10.3390/met14121428.

[60] S. Aksenov, V. Mikolaenko, 2025. Accurate determination of uniaxial flow behaviour of superplastic materials. Eur. J. Mech. A, Solids. 109, 105469. https://doi.org/10.1016/j.euromechsol.2024.105469.

[61] M. Böhnke, F. Kappe, M. Bobbert, G. Meschut, Influence of various procedures for the determination of flow curves on the predictive accuracy of numerical simulations for mechanical joining processes, Mater. Test. 63 (2021) 493–500. https://doi.org/10.1515/mt-2020-0082.

[62] C. Zhang, Y. Lou, 2023. Characterization and modelling of evolving plasticity behaviour up to fracture for FCC and BCC metals. J. Mater. Process. Technol. 317, 117997. https://doi.org/10.1016/j.jmatprotec.2023.117997.
[63] C. Zhang, Y. Lou, 2024. Influences of the evolving plastic behavior of sheet metal on V-bending and springback analysis considering different stress states. Int. J. Plast. 173, 103889. https://doi.org/10.1016/j.ijplas.2024.103889.
[64] S. Khoddam, S. Solhjoo, P.D. Hodgson, State of the art methods to post-process mechanical test data to characterize the hot deformation behavior of metals. Adv Mech Eng. 2021; 13 (11): https://doi.org/10.1177/16878140211061026.
[65] T. Matsuno, T. Fujita, T. Matsuda, Y. Shibayama, T. Hojo, I. Watanabe, 2023. Unstable stress-triaxiality development and contrasting weakening in two types of high-strength transformation-induced plasticity (TRIP) steels: Insights from a new compact tensile testing method. J. Mater. Process. Technol. 322, 118174. https://doi.org/10.1016/j.jmatprotec.2023.118174.
[66] B. Zhou, B. Guan, F. Han, X. Wu, M. Wan, 2025. A multiscale study on the novel strain hardening behavior of DP steels. Mater. Today Commun. 44, 111825. https://doi.org/10.1016/j.mtcomm.2025.111825.
[67] T. Matsuno, Y. Yamazaki, S. Matsubara, J. Eguchi, K. Shimizu, M. Koyama, Y. Okitsu, T. Tsuchiyama, Local Work-Hardening and Lüders Deformation Invariance in TRIP-Aided Medium-Mn High-Strength Steel: Significant TRIP Effect Changes in the Warm Temperature Range up to 200 °C, J. Jpn. Soc. Technol. Plast. 66 (2025). 61 – 68. https://doi.org/10.9773/sosei.240702.
[68] J. Wang, A. Pi, Z. Zhang, M. Wu, F. Huang, Z. Wang, F. Hao, 2025. A symmetric and asymmetric yield function based on normalized stress invariant suitable for sheet and bulk metals under various stress states. J. Mater. Process. Technol. 337, 118728. https://doi.org/10.1016/j.jmatprotec.2025.118728.
[69] O. Ibragimova, A. Brahme, W. Muhammad, D. Connolly, J. Lévesque, K. Inal, 2022. A convolutional neural network based crystal plasticity finite element framework to predict localised deformation in metals. Int. J. Plast. 157, 103374. https://doi.org/10.1016/j.ijplas.2022.103374.
[70] R. Esmaeilpour, H. Kim, T. Park, F. Pourboghrat, Z. Xu, B. Mohammed, F. Abu-Farha, Calibration of Barlat Yld2004-18P yield function using CPFEM and 3D RVE for the simulation of single point incremental forming (SPIF) of 7075-O aluminum sheet. Int. J. Mech. Sci. 145 (2018) 24-41. https://doi.org/10.1016/j.ijmecsci.2018.05.015.
[71] F. Han, M. Diehl, F. Roters, D. Raabe, 2020. Using spectral-based representative volume element crystal plasticity simulations to predict yield surface evolution during large scale forming simulations. J. Mater. Process. Technol. 277, 116449. https://doi.org/10.1016/j.jmatprotec.2019.116449.
[72] O. Engler, H. Aretz, 2021. A virtual materials testing approach to calibrate anisotropic yield functions for the simulation of earing during deep drawing of aluminium alloy sheet. Mater. Sci. Eng. A. 818, 141389. https://doi.org/10.1016/j.msea.2021.141389.
[73] K. Zhang, B. Holmedal, O.S. Hopperstad, S. Dumoulin, J. Gawad, A. Van Bael, P. Van Houtte, Multi-level modelling of mechanical anisotropy of commercial pure aluminium plate: crystal plasticity models, advanced yield functions and parameter identification. Int. J. Plast. 66 (2015) 3-30. https://doi.org/10.1016/j.ijplas.2014.02.003.
[74] H. Ma, Y. Li, H. Zhang, Q. Li, F. Chen, Z. Cui, 2022. A virtual laboratory based on full-field crystal plasticity simulation to characterize the multiscale mechanical properties of AHSS. Sci. Rep. 12, 5054. https://doi.org/10.1038/s41598-022-09045-8.

[75] S. Bouvier, H. Haddadi, P. Levée, C. Teodosiu, Simple shear tests: Experimental techniques and characterization of the plastic anisotropy of rolled sheets at large strains. J. Mater. Process. Technol. 172 (2006), 96–103. https://doi.org/10.1016/j.jmatprotec.2005.09.003.
[76] Y. Hou, J. Min, H.-R. Lee, J. Ha, N. Park, M.-G. Lee, 2024. A generalized, computationally versatile plasticity model framework - Part II: Theory and verification focusing on shear anisotropy. Int. J. Plast. 183, 104158. https://doi.org/10.1016/j.ijplas.2024.104158.
[77] N.J. Silk, M.R. van der Widen, Interpretation of hot plane strain compression testing of aluminium specimens, J. Mater. Sci. Technol. 5 (1999) 295-300.
[78] B. Kowalski, C.M. Sellars, M. Pietrzyk, Identification of rheological parameters on the basis of plane strain compression test on specimens of various initial dimensions, Comput. Mater. Sci. 35 (2006) 92-97. https://doi.org/10.1016/j.commatsci.2005.02.024.
[79] C. Slater, N. Tamanna, C. Davis, 2021. Optimising compression testing for strain uniformity to facilitate microstructural assessment during recrystallisation. Results in Materials. 11, 100218. https://doi.org/10.1016/j.rinma.2021.100218.
[80] M. Pietrzyk, J.G. Lenard, G.M. Dalton, A Study of the Plane Strain Compression Test. CIRP Annals. 42 (1993) 331-334. https://doi.org/10.1016/S0007-8506(07)62455-X.
[81] S. Aksenov, J. Kliber, Y. Puzino, S. Bober, Processing of plane strain compression test results for investigation of AISI-304 stainless steel constitutive behavior, J. Chem. Technol. Metall. 50 (2015) 644–650.
[82] N. Becker, K. Pöhlandt, K. Lange, Improvement of the Plane-Strain Compression Test for Determining Flow Curves, CIRP Ann.-Manuf. Technol. 38 (1989) 227–230. https://doi.org/10.1016/S0007-8506(07)62691-2.
[83] C. Chermette, K. Unruh, I. Peshekhodov, J. Chottin, T. Balan, A new analytical method for determination of the flow curve for high-strength sheet steels using the plane strain compression test, Int. J. Mater. Form. 13 (2020) 269-292. https://doi.org/10.1007/s12289-019-01485-4.
[84] A. Gavrus, E. Massoni, J.L. Chenot, An inverse analysis using a finite element model for identification of rheological parameters, J. Mater. Process. Technol. 60 (1996) 447–454. https://doi.org/10.1016/0924-0136(96)02369-2.
[85] G. Capilla, H. Hamasaki, F. Yoshida, Determination of uniaxial large-strain workhardening of high-strength steel sheets from in-plane stretch-bending testing, J. Mater. Process. Technol. 243 (2017) 152–169. http://dx.doi.org/10.1016/j.jmatprotec.2016.12.002.
[86] Ruibin Mei, Li Bao, Tanqiu Chen, Lihao Chen, Xianghua Liu, Discussion on stress assumption and yield criterion determination rule in teaching of the PSM, J. Braz. Soc. Mech. Sci. Eng. 47 (2025) 1-11. https://doi.org/10.1007/s40430-024-05342-7.
[87] G. Venet, T. Balan, C. Baudouin, R. Bigot, Direct usage of the wire drawing process for large strain parameter identification, Int. J. Mater. Form. 12: (2019) 875–888. https://doi.org/10.1007/s12289-018-01458-z.
[88] H. Ismar, O. Mahrenholtz, Technische Plastomechanik. Fried. Vieweg& Sohn, Braunschweig/Wiesbaden, Germany, 1978, 112–125.
[89] S. Coppieters, H. Traphöner, F. Stiebert, T. Balan, T. Kuwabara, A.E. Tekkaya, 2022. Large strain flow curve identification for sheet metal. J. Mater. Process. Technol. 308, 117725. https://doi.org/10.1016/j.jmatprotec.2022.117725.
[90] M.P.F. Sutcliffe, P. Montmitonnet, Numerical modelling of lubricated foil rolling. Revue de Metallurgie, Cahiers D'Informations Techniques. 98 (2001) 435–442. https://doi.org/10.1051/metal:2001197.
[91] J. Kubié, F. Delamare, Mécanique des solides anélastiques, Comptes Rendus de l'Académie des Sciences. 291 (1980) 97–100.

[92] J.C. Gelin, O. Ghouati, R. Shahani, Modelling the plane strain compression test to obtain constitutive equations of aluminium alloys, Int. J. Mech. Sci. 36 (1994) 773–796. https://doi.org/10.1016/0020-7403(94)90009-4.